

**The Near Infrared and Multiwavelength Afterglow of GRB 000301c**

James E. Rhoads

and

Andrew S. Fruchter

*Space Telescope Science Institute***ABSTRACT**

We present near-infrared observations of the counterpart of GRB 000301c. The K' filter ( $2.1\ \mu\text{m}$ ) light curve shows a well-sampled break in the decay slope at  $t \approx 3.5$  days post-burst. The early time slope is very shallow ( $\sim -0.1$ ), while the late time slope is steep ( $-2.2$ ). Comparison with the optical (R band) light curve shows marginally significant differences, especially in the early time decay slope (which is steeper in the optical) and the break time (which occurs *later* in the optical). This is contrary to the general expectation that light curve breaks should either be achromatic (e.g., for breaks due to collimation effects) or should occur later at longer wavelengths (for most other breaks). The observed color variations might be intrinsic to the afterglow, or might indicate systematic errors of  $\gtrsim 0.08$  magnitude in all fluxes. Even if the break is achromatic, we argue that its sharpness poses difficulties for explanations that depend on collimated ejecta. The R light curve shows further signs of fairly rapid variability (a bump, steep drop, and plateau) that are not apparent in the K' light curve. In addition, by combining the IR-optical-UV data with millimeter and radio fluxes, we are able to constrain the locations of the self-absorption break and cooling break and to infer the location of the spectral peak at  $t = 3$  days,  $f_\nu \approx 3.4$  mJy at  $\nu \approx 10^{12}$  Hz. Using the multiwavelength spectral energy distribution, we are able to constrain the blast wave energy, which was  $E \gtrsim 3 \times 10^{53}$  erg if the explosion was isotropic. This implies a maximum gamma ray production efficiency of  $\sim 0.15$  for GRB 000301C.

*Subject headings:* Gamma rays—bursts

**1. Introduction**

Infrared observations can be used to improve our understanding of gamma ray burst afterglows in several ways. First, they can be combined with optical measurements to obtain spectral slope measurements with a much wider wavelength baseline, and hence yield a more accurate spectral

slope than optical data alone. Second, they can be used to test observed light curve breaks for wavelength dependence, which is an important discriminant between breaks due to ejecta collimation and other possible causes. Finally, it has been suggested that bursts are preferentially located in dusty regions, e.g., under “hypernova” scenarios where bursters are a final evolutionary stage of some class of massive stars. If so, and if the dusty region extends beyond the expected dust destruction distance (Waxman & Draine 1999), then near-infrared observations will detect some afterglows that are obscured at optical wavelengths. At less extreme dust optical depths, near-infrared data help to characterize the host galaxy extinction and so infer both extinction corrected fluxes and properties of dust and gas in high redshift GRB host galaxies.

We present here near-infrared (NIR) photometric observations of the afterglow of the gamma ray burst GRB 000301c. These constitute the best-sampled near infrared light curve for any afterglow to date.

GRB 000301c was detected independently by the All-Sky Monitor on the Rossi X-Ray Timing Explorer and by two spacecraft (Ulysses and NEAR) of the current Interplanetary Network on 2000 March 1.4108 UT. The event was a single peaked GRB lasting approximately 10 seconds (Smith, Hurley, & Cline 2000) at low energies ( $< 10$  keV) and 2 seconds at higher energies ( $> 25$  keV) (Jensen et al 2000). Coordinates were available approximately 36 hours after the burst, and an optical counterpart was reported by Fynbo et al (2000) based on observations at March 3.21 UT. The redshift of the burst was first reported as  $z = 1.95 \pm 0.1$  (Smette et al 2000a) and subsequently refined to  $z = 2.028 \pm 0.025$  (Smette et al 2000b) using the observed Lyman break in a near-UV spectrum of the GRB afterglow. Weak metal lines in absorption yielded further improvements to  $z = 2.0335 \pm 0.0003$  (Castro et al 2000) or  $z = 2.0404 \pm 0.0008$  (Jensen et al 2000).

## 2. Photometric Data

### 3. Infrared Telescope Facility Images

We present data obtained at the NASA Infrared Telescope Facility (IRTF) on Mauna Kea as part of a service mode Target of Opportunity program for broadband near-IR followup of gamma ray bursts using the NSFCam imager. Observing conditions were good throughout the period, with clear skies and subarcsecond seeing on all nights. All data were taken with a plate scale of  $0.3''$  per pixel. A log of the observations is given in table 1.

We reduced and analyzed the data following standard near-IR procedures. Raw sky flats were generated for each filter and night using the mean of all available frames after outlier rejection to eliminate the influence of objects on the flatfield. Final flats were generated by subtracting stacked dark frames (taken with the same exposure time, number of coadds, and number of nondestructive reads as the data) from the raw flats and normalizing the result to have mean = 1. Individual frames were then sky-subtracted (using the median of three to six frames taken immediately before

and/or after the object frame) and flatfielded. Frames were aligned using bilinear interpolation to implement a simple shift based on the measured centroid of a bright star. Finally, the aligned frames were combined using a clipped mean after removing any sky subtraction residuals through subtraction of the modal pixel value.

We measured the GRB fluxes on all nights using aperture photometry with an aperture diameter of  $1.8''$ . All afterglow photometry was taken relative to the bright star  $5.7''$  west and  $1''$  south of the optical transient. (This is star A of Garnavich et al 2000a.) The J and K' band magnitudes of this star were  $J_{\text{CIT}} = 16.64 \pm 0.01$  and  $K' = 15.97 \pm 0.02$ . These were calibrated using observations of UKIRT faint standard 27 (FS27, Casali & Hawarden 1992) taken immediately before the first IRTF observations of GRB 000301c. The reference magnitudes used for FS 27 were  $K' = 13.14$  (based on photometric transformation equations from Wainscoat & Cowie 1992) and  $J_{\text{CIT}} = 13.45$  (based on equations from the NSFCam documentation). The standard star observations were processed in the same way as the GRB images, and a larger photometry aperture ( $5.4''$  diameter) was used for flux calibration, to reduce sensitivity to any centering errors or seeing variations between the standard star and GRB frames. No correction was made for atmospheric extinction; however, any such correction would be small ( $\lesssim 0.01$  mag), because the standard was observed at airmass 1.09, and the GRB field at airmass 1.02. The reference star showed no evidence for variability either in our near-IR data or in optical data from two groups (Garnavich, private communication; Halpern, private communication). The aperture photometry included a local sky estimation and subtraction using the mode of pixel values in an annulus around each point source. This step should control any residual sky level or first order gradient in the sky. Moreover, by selecting the annulus to avoid bright objects and using the mode for sky level estimation, we also control the possible influence of other sources on sky level estimates.

Our counts always remained below the nominal linearity limit for NSFCam (Leggett & Denault 1996); we therefore did not apply nonlinearity corrections to our data. We placed the J band data on the CIT magnitude system using  $J_{\text{CIT}} = J_{\text{MK}} - 0.01(J - K)$ , where  $J_{\text{MK}}$  is the natural magnitude system for the current Mauna Kea J filter in NSFCam. This gives  $J_{\text{CIT}} = 19.11$  for the afterglow on March 4.652. The K' magnitudes were left on the NSFCam instrumental system.

Errors due to photon counting statistics were computed based on an iteratively clipped variance of each night's final stacked images, suitably corrected for the correlated noise introduced by bilinear interpolation. Sky subtraction errors arise only from the difference between sky level in the photometry aperture and in the sky annulus. These errors are separated into statistical errors (due to photon noise in the sky annulus) and systematic (due to objects in the sky annulus or any other source of bias in estimating the true background under the transient source). The statistical part is always small compared to statistical errors from the object flux measurement, due to the large number of pixels in the sky annulus ( $\sim 900$ ) and much smaller number ( $\sim 28$ ) in the photometric aperture. Systematic errors in sky subtraction are potentially larger, but we believe they are under reasonable control in our data set because the sky level was removed in two steps (globally, during data reduction, and locally, during aperture photometry) accounting for up to first order gradients

in both time and space; and because the weather was cooperative, with relatively little temporal variation in sky background ( $< 10\%$  minimum to maximum in any night and filter, and usually less) and subarcsecond seeing (allowing small photometry apertures). Further possible error sources include centroiding of the afterglow and reference star (expected to be systematic-error limited at the 0.1 pixel level) and residual flatfielding difficulties. Neither will be large compared to our photon counting noise. To be conservative, we estimate that sky subtraction and flatfielding errors combined may affect all of our photometry at up to the 4% level. Table 1 lists both pure photon counting errors and error bars including this systematic error added in quadrature.

### 3.1. Data from Other Sources

In addition to the IRTF data, we include in our analysis data from other observatories presented in the literature (both the GRB Coordinate Network Circulars and preprints by Masetti et al 2000 and Jensen et al 2000). These data are summarized in table 2. For data points reported multiple times, we use the most recently reported value. In particular, for the Uttar Pradesh State Observatory data we take values from Masetti et al (2000) rather than Sagar et al (2000).

Two early time K' data points come from Calar Alto data of Stecklum et al (2000) and Subaru data of Kobayashi et al (2000a,b). Flux values from both were measured relative to the Garnavich et al (2000a) star A. The use of a uniform reference star allows the data from multiple observatories to be compared with reasonable confidence. Residual differences in color terms should be small since all three observatories used the same photometric bandpass. To allow for color terms, we have used  $\sigma = 0.03$  mag as the effective error on the Subaru data, rather than the photometric error 0.01 mag reported by Kobayashi et al (2000a,b).

Similarly, the optical data reported in the literature and used in this paper has all been calibrated to either stars A-D of Garnavich et al (2000a) (for some R band data) or to the photometry of Henden et al (2000) (for other optical filters and the rest of the R band data). The R band fluxes measured by Henden et al for stars A-D agree with those from Garnavich et al within the uncertainties, which are  $\sim 5\%$ . The mean and median magnitude differences between the two calibrations are 0.050 and 0.036 magnitude respectively, in the sense that Garnavich et al report brighter magnitudes than do Henden et al. The possibility of inconsistent photometric zero points in different data sets therefore amounts to about 0.05 magnitude between authors using calibrations from the two alternative sources, and less for authors using the same calibration. The two largest sets of uniformly reduced optical data currently available are Masetti et al (2000) and Jensen et al (2000). Both groups use the Henden et al calibration. We have increased all R band fluxes reported on the Garnavich et al (2000a) zero point by 0.04 magnitude to adjust all R band photometry to the Henden et al (2000) zero point.

Another possible systematic difference between photometry from different observatories is color term differences. To estimate the importance of these effects, we compare the magnitude difference

between the GRB afterglow and a comparison star for thick and thinned CCD chips behind a standard Cousins R filter (Bessell 1990). The quantum efficiency of a thick chip was approximated by  $QE = 0.45 + (\lambda/\mu m - 0.65)$ , and that of a thin chip by  $QE = 0.85 - 0.8(\lambda/\mu m - 0.65)$ . (Both these relations are approximations based on plots from the Steward Observatory CCD Lab web pages and valid for the R band spectral region.) We take the afterglow spectrum to be a power law with  $f_\nu \propto \nu^{-1}$  (a characteristic value for this afterglow before any reddening corrections; see below), and take stellar spectral energy distributions from Gunn and Stryker (1983). The result depends on the color of the comparison star. For stars with the colors of unreddened G0 to K4 dwarfs (which includes stars A and D of Garnavich et al 2000a), the difference in inferred magnitude for the two  $QE(\lambda)$  models is  $\leq 0.01$  magnitude. For redder or bluer stars, the differences can be substantial: Up to 0.05 magnitude for O stars, 0.07 magnitude for M0 stars (approximately matching Garnavich et al’s stars B and C), and 0.20 magnitude for the coolest M stars. However, only 9% of stars in the Henden et al list are redder than stars B and C. Overall, then, color terms will be a modest source of error (no greater than the random photometric error and the zero point error) except for pathological choices of comparison stars. Jensen et al (2000) explicitly address this issue by using comparison stars of color similar to the GRB afterglow in their analysis.

A final possible source of error arises from possible “crowded field” effects in the photometry. Star A is located  $6''$  from the GRB afterglow. With sufficiently poor seeing, aperture photometry of the afterglow might be affected by the wings of this star’s point spread function (PSF). We have estimated the magnitude of this error as a function of aperture size and seeing through numerical calculations with a Gaussian PSF model. We find that photometric errors from this source are negligible ( $\ll 0.01$  mag) for seeing better than  $2''$  (FWHM). They remain  $\leq 0.015$  mag even for  $3''$  seeing provided that the photometric aperture radius used is  $\leq 1.8''$ . PSF-fitting photometry, as done by Masetti et al (2000) and Jensen et al (2000), is more robust to such errors.

The ultraviolet flux at  $0.28 \mu m \leq \lambda \leq 0.33 \mu m$  is taken from the continuum level in the Hubble Space Telescope STIS spectrum of the afterglow (Smette et al 2000b). This measurement was  $f_\lambda = (7.3_{-1.8}^{+0.8} \pm 0.6) \times 10^{-18} \text{ erg cm}^{-2} \text{ s}^{-1} \text{ \AA}^{-1}$ . The dominant (first) error bar comes from uncertainties in wavelength calibration coupled with strongly wavelength-dependent sensitivity; the second error bar is a random error. This corresponds to  $f_\nu(0.305 \mu m) = (2.26_{-0.56}^{+0.25} \pm 0.19) \mu\text{Jy}$ . Over this wavelength range,  $f_\lambda$  is approximately constant, so  $f_\nu \sim \nu^{-2}$ . This slope is steeper than the optical-IR slopes derived in section 6 below, but is consistent with a wavelength independent intrinsic slope if intergalactic Lyman line absorption is considered (Madau 1995).

UT Date	$t$	Filter	Exposure (seconds)	Number of Frames	Seeing	Magnitude	Error (photometric)	Error (total)
4.652	3.241	J	700	14	0.95''	19.11	0.05	0.064
4.640	3.229	K'	672	14	0.85''	17.66	0.04	0.057
5.610	4.199	K'	672	14	0.69''	18.01	0.05	0.064
6.595	5.184	K'	435	9	0.71''	18.57	0.12	0.126
8.590	7.179	K'	1400	28	0.68''	19.29	0.09	0.098

Table 1: Log of the IRTF data.  $t$  is the observed time elapsed since the GRB. “Exposure” is the sum of the exposure times for all GRB images in that filter and night. The “photometric” error is due to poisson statistics of received photons. The “total” error combines the photometric error in quadrature with an estimated 0.04 magnitudes error due to sky subtraction and flatfielding uncertainties.

Table 2. Data from the literature.

UT Date	$t$	Filter	Magnitude	Authors	Reference
3.215	1.804	K'	$17.52 \pm 0.06$	Stecklum et al	GCNC 572 & private communication
3.55	2.14	K'	$17.53 \pm 0.03$	Kobayashi et al	GCNC 577, 587
4.640	3.229	K'	$17.66 \pm 0.057$	Rhoads & Fruchter	This work
5.610	4.199	K'	$18.01 \pm 0.064$	Rhoads & Fruchter	This work
6.595	5.184	K'	$18.57 \pm 0.126$	Rhoads & Fruchter	This work
8.590	7.179	K'	$19.29 \pm 0.098$	Rhoads & Fruchter	This work
3.55	2.14	J	$18.91 \pm 0.03$	Kobayashi et al	GCNC 577, 587
4.652	3.241	J	$19.11 \pm 0.064$	Rhoads & Fruchter	This work
2.906	1.495	R	$20.42 \pm 0.04$	Masetti et al	A
2.961	1.550	R	$20.02 \pm 0.03$	Bhargavi & Cowsik	GCNC 630
3.14	1.729	R	$20.09 \pm 0.04$	Jensen et al	B
3.144	1.733	R	$20.25 \pm 0.05$	Masetti et al	A
3.17	1.759	R	$20.15 \pm 0.04$	Jensen et al	B
3.185	1.774	R	$20.16 \pm 0.05$	Masetti et al	A
3.19	1.779	R	$20.11 \pm 0.04$	Jensen et al	B
3.205	1.794	R	$20.25 \pm 0.05$	Masetti et al	A
3.21	1.799	R	$20.14 \pm 0.04$	Jensen et al	B
3.25	1.839	R	$20.16 \pm 0.04$	Jensen et al	B
3.51	2.10	R	$20.32^\dagger \pm 0.05$	Garnavich et al	GCNC 573
3.51	2.10	R	$20.27 \pm 0.04$	Veillet et al	GCNC 575, 588
3.51	2.10	R	$20.28^\dagger \pm 0.05$	Halpern et al	GCNC 578
3.913	2.502	R	$20.51 \pm 0.04$	Masetti et al	A
3.998	2.587	R	$20.49 \pm 0.10$	Bhargavi & Cowsik	GCNC 630
4.038	2.627	R	$20.53 \pm 0.06$	Masetti et al	A
4.080	2.669	R	$20.613^\dagger \pm 0.06$	Gal-Yam et al	GCNC 593
4.38	2.97	R	$20.60^\dagger \pm 0.05$	Garnavich et al	GCNC 581
4.42	3.01	R	$20.61 \pm 0.06$	Jensen et al	B
4.458	3.047	R	$20.58^\dagger \pm 0.06$	Mujica et al	GCNC 597
4.48	3.069	R	$20.58 \pm 0.03$	Jensen et al	B
4.49	3.079	R	$20.54 \pm 0.04$	Jensen et al	B
4.50	3.089	R	$20.60 \pm 0.04$	Jensen et al	B
4.50	3.09	R	$20.65^\dagger \pm 0.04$	Halpern et al	GCNC 582
4.909	3.498	R	$20.58 \pm 0.05$	Bhargavi and Cowsik	GCNC 630

#### 4. Light curve fitting

Both the K' and R light curves are shown in figure 1. The K' band light curve shows a smooth rollover from an initially constant flux to a rapid decay at late time. The R band light curve shows a qualitatively similar behavior, but the early time R flux decays more steeply than the early K' flux, and there are additional irregularities in the R band light curve that are arguably significant (e.g., Masetti et al 2000; Sagar et al 2000).

Broken power laws can be empirically fitted by functions of the form  $f = f_0 [(t/t_b)^{\alpha_1\beta} + (t/t_b)^{\alpha_2\beta}]^{-1/\beta}$ . With  $\alpha_1 < \alpha_2$  and  $\beta > 0$ , this function describes a light curve falling as  $t^{-\alpha_1}$  at  $t \ll t_b$  and  $t^{-\alpha_2}$  at  $t \gg t_b$ .  $\beta$  controls the sharpness of the break, with larger  $\beta$  implying a sharper break. The function that Stanek et al (1999) used to fit the light curve of GRB 990510 is the special case  $\beta = 1$  of this function. Rewritten in magnitudes, the fitting function becomes

$$m = m_b + \frac{2.5}{\beta} \left\{ \log_{10} \left[ (t/t_b)^{\alpha_1\beta} + (t/t_b)^{\alpha_2\beta} \right] - \log_{10}(2) \right\} \quad (1)$$

where  $m_b$  is the magnitude at time  $t_b$ .

The K' light curve can be well fitted by this model. The best fit values (with  $\chi^2 = 0.422$  for one degree of freedom [d.o.f]) are  $t_b = 3.57$  days,  $K_b = 17.76$ ,  $\alpha_1 = 0.09$ ,  $\alpha_2 = 2.26$ , and  $\beta = 4.23$ .

The R band data show significant departures from such a light curve. The first R band data point is clearly fainter than the extrapolation of the other early R data. If we exclude this point, the best fit to the R data has  $\chi^2/\text{d.o.f} = 2.8$  for 41 degrees of freedom. This fit has  $t_b = 5.1$  days,  $R_b = 21.18$ ,  $\alpha_1 = 0.69$ ,  $\alpha_2 = 2.77$ , and  $\beta = 3.2$ . (Including the earliest point gives instead  $\chi^2/\text{d.o.f} \approx 4.7$ , with  $t_b = 4.97$  days,  $R_b = 21.15$ ,  $\alpha_1 = 0.56$ ,  $\alpha_2 = 2.81$ , and  $\beta = 2.25$ .) The largest deviations from the smooth light curve (aside from the first data point) are from the bump at  $t \approx 3.75$  days, the plateau at  $\lesssim t \lesssim 7$  days, and the steep decline between the two. We believe all three are likely real features. This behavior may indicate variations in the external medium density (see Kumar & Panaitescu 2000b) or refreshed shock effects (Panaitescu, Meszaros, & Rees 1998; Dai & Lu 2000). Either explanation suggests that the K' data should show similar effects. To test this, we examine the behavior of  $R - K'$  below.

If we assume a fixed  $R - K'$  color and compare the  $K'$  data to the R band light curve model, the best fit color is  $R - K' = 2.80$  and  $\chi^2/\text{d.o.f} = 6.6$  for 5 degrees of freedom (6 data points - 1 color). The same time interval includes about half the R data (31 points), and the data - model residuals in R yield  $\chi^2/\text{d.o.f} = 3.9$ . This relatively large  $\chi^2$  is due to the presence of the bump, drop, and plateau in this time interval. In short, the smooth R band fit does not describe the R data very well in this time period, but does an even worse job describing the K' data.



Table 2—Continued

UT Date	$t$	Filter	Magnitude	Authors	Reference
5.135	3.724	R	$20.47 \pm 0.07$	Masetti et al	A
5.39	3.979	R	$20.61 \pm 0.05$	Jensen et al	B
5.63	4.22	R	$20.86 \pm 0.04$	Veillet et al	GCNC 588
5.930	4.519	R	$21.14 \pm 0.06$	Masetti et al	A
6.135	4.724	R	$21.65 \pm 0.20$	Masetti et al	A
6.22	4.81	“R”	$21.5 \pm 0.15$	Fruchter et al	GCNC 602
6.39	4.98	“R”	$21.43 \pm 0.26$	Jensen et al	B
7.125	5.714	R	$21.68 \pm 0.15$	Masetti et al	A
7.22	5.809	R	$21.59 \pm 0.07$	Jensen et al	B
7.65	6.24	R	$21.70 \pm 0.07$	Veillet et al	GCNC 598
7.894	6.483	R	$22.00 \pm 0.15$	Masetti et al	A
8.146	6.735	R	$21.68 \pm 0.10$	Masetti et al	A
8.18	6.769	R	$21.80 \pm 0.05$	Jensen et al	B
8.924	7.513	R	$22.04 \pm 0.20$	Masetti et al	A
9.15	7.739	R	$22.11 \pm 0.15$	Jensen et al	B
9.52	8.11	R	$22.32^\dagger \pm 0.09$	Halpern & Kemp	GCNC 604
11.39	9.979	R	$23.12 \pm 0.18$	Jensen et al	B
11.63	10.22	R	$23.02 \pm 0.10$	Veillet et al	GCNC 610
12.44	11.03	R	$23.10 \pm 0.22$	Jensen et al	B
14.60	13.19	R	$23.82 \pm 0.10$	Veillet et al	GCNC 611
34.9	33.5	“R”	$26.5 \pm 0.15$	Fruchter et al	GCNC 627, 701
50.0	48.59	“R”	$27.9 \pm 0.15$	Fruchter et al	GCNC 701
3.50	2.09	B	$21.11 \pm 0.04$	Veillet et al	GCNC 575,588
4.52	3.11	B	$21.41 \pm 0.04$	Halpern et al	GCNC 585
14.60	13.19	B	$24.83 \pm 0.12$	Veillet et al	GCNC 611
6.714	5.303	UV	$2.26^{+0.31}_{-0.59} \mu\text{Jy}$	Smette et al	C
4.385	2.974	1.2mm	$2.1 \pm 0.3 \text{ mJy}$	Berger et al	D
5.67	4.26	1.33cm	$884 \pm 216 \mu\text{Jy}$	Berger et al	D
5.67	4.26	3.54cm	$316 \pm 41 \mu\text{Jy}$	Berger et al	D
5.67	4.26	6.17cm	$240 \pm 53 \mu\text{Jy}$	Berger et al	D
5.67	4.26	20.9cm	$11 \pm 79 \mu\text{Jy}$	Berger et al	D

Note. — The estimated error on Kobayashi et al data has been increased from their 0.01 magnitude statistical error to 0.03 mag to allow for possible color terms in conversion between their photometric system and ours. R band magnitudes flagged with “†” were originally reported with calibration from Garnavich et al (GCNC 573) and are here adjusted by +0.04 mag to place them on the flux zero point of Henden et al (GCNC 583). Four measurements use “pseudo-R” filters: Three of these (from Fruchter et al) are HST STIS unfiltered data, and one (from Jensen et al) is from VLT spectrophotometry; both are calibrated to R band. References are either GRB Coordinate Network Circular numbers, or preprints coded as follows: A: Masetti et al 2000, to appear in A&A, astro-ph/0004186v2; B: Jensen et al 2000, submitted to A&A, astro-ph/0005609; C: Smette et al 2000, submitted to ApJ, astro-ph/0007202; D: Berger et al, to appear in ApJ, astro-ph/0005465.

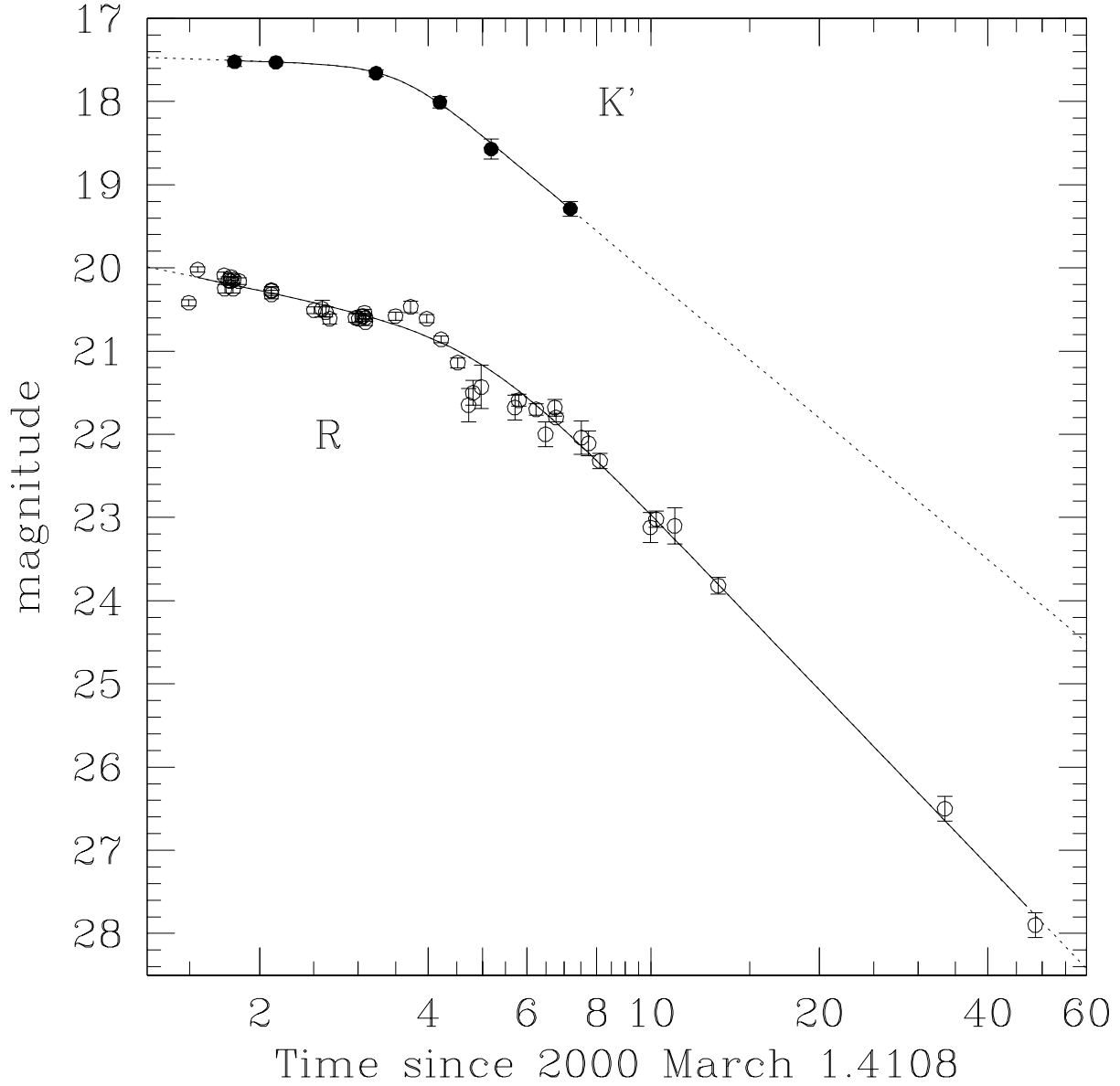


Fig. 1.— The light curves of the GRB 000301c afterglow in both K' and R filters. The data are summarized in table 2. Smoothly broken power law fits using the empirical fitting form in equation 1 are shown as solid lines where they interpolate the data, and as dotted lines where they are extrapolations. The fitted parameters are given in the text. Filled circles are K' filter data and open circles are R filter data.

## 5. $R - K'$ color variations

To assess the significance of the light curve fit differences above, we have examined in detail the  $R - K'$  colors of the afterglow for the six  $K'$  data points. At each epoch, we use selected  $R$  data points to obtain the most reliable interpolated or extrapolated  $R$  flux at the time of the  $K'$  measurement. All measurements are adjusted to the zero point of Henden et al (2000). Details for each epoch follow.

March 3.215: We interpolate between the March 3.21 and March 3.25 Nordic Optical Telescope measurements by Jensen et al (2000), obtaining  $R = 20.145 \pm 0.04$ . Hence,  $R - K' = 2.62 \pm 0.07$ .

March 3.55: We take a weighted average of the three measurements from March 3.51 (Garavich et al 2000a; Halpern et al 2000a; Veillet et al 2000a,b). We apply corrections to place the first two epochs on the Henden et al zero point, and further add 0.02 magnitudes to adjust the  $R$  flux to the  $K'$  epoch, one hour later. (This corresponds to a local  $t^{-1}$  decay.) We obtain  $R = 20.32 \pm 0.04$  and  $R - K' = 2.79 \pm 0.05$ .

March 4.64: We combine four  $R$  measurements from March 4.48 to 4.50 (three from Jensen et al 2000; one from Halpern et al 2000b, adjusted by 0.05 mag to the Henden et al zero point) and interpolate to the March 4.909 point of Bhargavi & Cowsik to obtain  $R = 20.59 \pm 0.04$ . Hence,  $R - K' = 2.93 \pm 0.06$ .

March 5.61: We extrapolate the March 5.63  $R$  band point from Veillet et al (2000) to the  $K'$  epoch, obtaining  $R = 20.85 \pm 0.04$  and  $R - K' = 2.84 \pm 0.06$ .

March 6.595: This epoch is during the “plateau” in the  $R$  band light curve (Bernabei et al 2000). Fitting a single power law through the  $R$  data from March 6.135 to March 7.22, evaluating it at March 6.595, and estimating the flux error through Monte Carlo simulations, we find  $R = 21.57 \pm 0.07$ . The resulting color is  $R - K' = 3.00 \pm 0.14$ . This color does depend on our assessment that the “plateau” is a real feature. If we extend the fit to earlier times (starting at March 5.93), the color becomes 0.14 mag bluer, though a single power law fit does not describe the data well over the full period from March 5.93 to March 7.22.

March 8.590: We use the  $R$  data from March 8.146 through 9.52. We again fit a single power law decay through all the  $R$  data, evaluate it at the epoch of the  $K'$  measurement, and determine the error bar from simulations. The result is  $R = 21.95 \pm 0.04$ , so that  $R - K' = 2.66 \pm 0.10$ .

These values of  $R - K'$  are plotted as a function of time in figure 2. If we assume a single  $R - K'$  color throughout the afterglow, the best fit is  $R - K' = 2.79$ . With  $\chi^2/\text{d.o.f} = 2.87$  for 5 degrees of freedom, this fit is not especially good.

We consider three possible explanations for the observed variation of  $R - K'$  with time. First, it is possible that the color variations are real. Second, as suggested by Masetti et al (2000), it may be that there are no true color variations, but that the afterglow exhibits achromatic fluctuations on time scales short compared to the interval between observations. If so, the fluctuations need

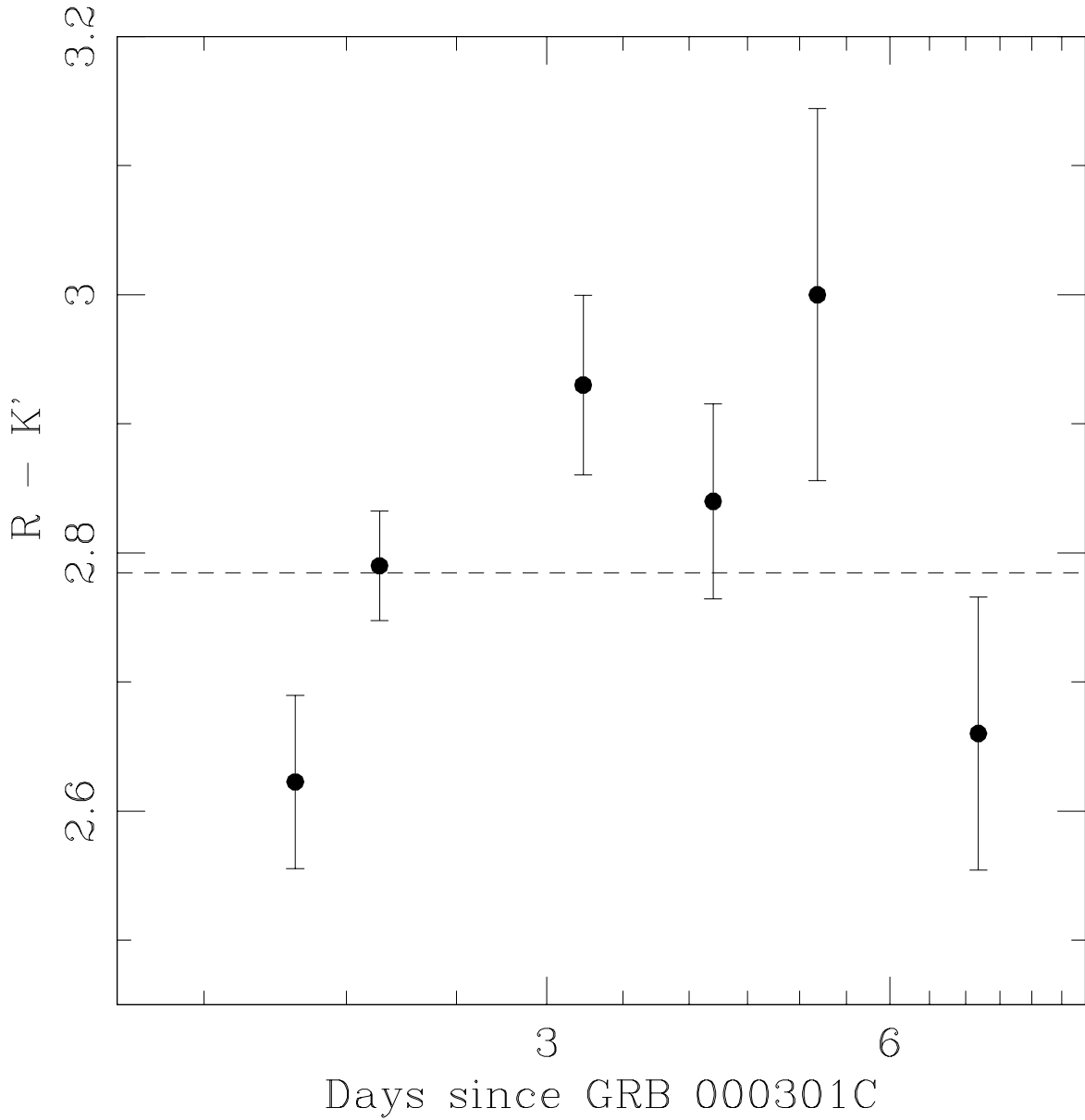


Fig. 2.— The  $R - K'$  color evolution of the GRB 000301c afterglow. The dashed line shows the best fit single color,  $R - K' = 2.78$ . Each epoch is a direct  $K'$  measurement and an interpolated  $R$  flux.

to have amplitude  $\sim 10\%$  and to occur on timescales  $\delta t \lesssim 3.3 \text{ hours} = 0.04t$  to explain the March 4.64 data, and  $\delta t \sim 7 \text{ minutes} = 0.003t$  to explain the March 3.21 data. The latter in particular is physically implausible for an afterglow expanding into a realistic external medium. Finally, if the error bars on the photometry are systematically underestimated, the data may be reconciled with no color evolution. In order to reduce  $\chi^2$  to 5 (so that  $\chi^2/\text{dof} = 1$ ), we need to add a systematic error contribution of 0.078 magnitudes in quadrature to all of the  $K'$  and interpolated  $R$  fluxes. Given the discussion of systematic errors above and our effort to adjust all  $R$  band fluxes to the Henden et al calibration, this large an additional error is unlikely. We therefore believe that at least some of the measured color variation is real.

## 6. Spectral Energy Distributions

The long spectral baseline between the  $K'$  band ( $2.1 \mu\text{m}$ ) and the optical/UV bands allows one to obtain accurate spectral slope measurements. We have calculated the burst spectral energy distribution at selected times based on the availability of multiwavelength data. Where necessary, flux measurements were interpolated between adjacent data points at one wavelength in order to determine a contemporaneous flux with another wavelength. For this operation, we always interpolated the light curves with good sampling ( $R$ ,  $K'$ ) to match the time of a sparsely sampled wavelength (UV 2825Å, B). Photometric zero points for the conversion of magnitudes to flux density units were taken from Fukugita, Shimasaku, & Ichikawa (1995) for the optical, and from Campins, Rieke, & Lebofsky (1985) for the near-IR.

The resulting spectral energy distributions are shown in figure 3. The best-fit spectral slopes assuming unbroken power law spectra are given in table 3, first uncorrected for extinction; then with a correction for foreground Galactic extinction ( $E_{B-V} = 0.053$ , Schlegel et al 1998) assuming an  $R_V \equiv A_V/E_{B-V} = 3.1$  extinction law; and finally with an additional correction for possible extinction in the GRB host galaxy (see below). Also included are the slopes derived from  $R$  and  $K'$  data alone, corrected only for Galactic extinction.

The broad band spectral energy distributions plotted in figure 3 show no compelling evidence for extinction at the redshift of the GRB. (This is a change from the first preprint of this paper, largely due to revised calibration of the March 6.375 UV data point at 3050Å.) However, a modest amount of host galaxy extinction remains consistent with the data.

The 2175Å dust absorption feature falls into the observed  $R$  band at the redshift  $z = 2.03$  of this burst. Assuming that there is no intrinsic emission feature at this wavelength in the GRB afterglow spectrum, we can place an upper limit of  $A_V \lesssim 0.1$  magnitude for Milky Way type dust at  $z = 2.03$ . Dust with a different reddening law is less strongly constrained. A Small Magellanic Cloud reddening law is plausible for  $A_V \lesssim 0.12$ , while a Large Magellanic Cloud (LMC) law is plausible for  $A_V \lesssim 0.2$ . The measure of plausibility here is that a single power law should approximately fit the spectrum at any given epoch. As an illustrative case, we have shown in figure 3 the spectral

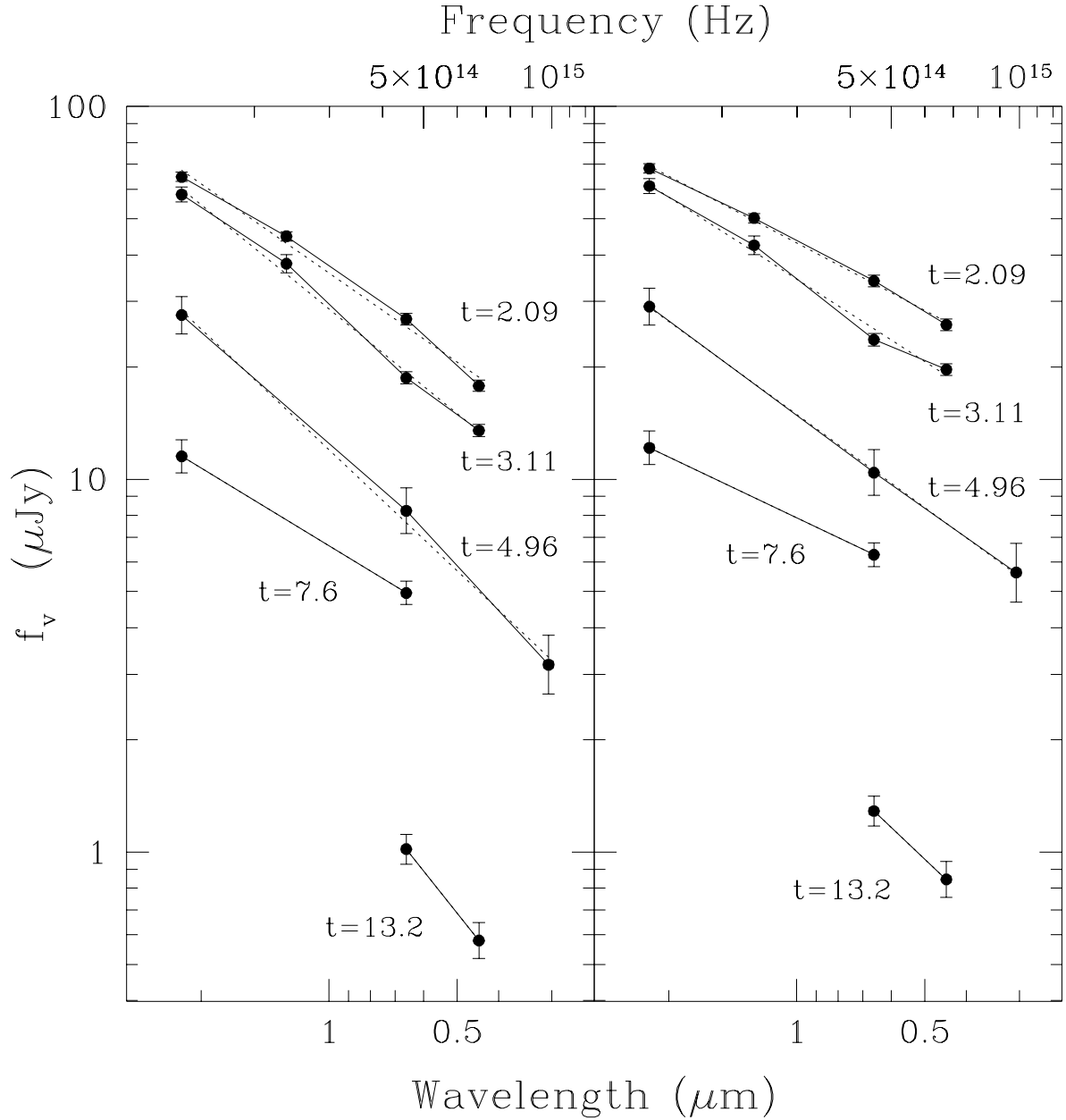


Fig. 3.— The spectral energy distribution of the GRB 000301c afterglow in the observer-frame near-IR to near-UV is plotted for selected epochs. Left panel: Spectral energy distributions (SEDs) corrected for Galactic extinction only. Note the slight but significant curvature of the SED at the earliest epoch, when the errors are smallest. Right panel: An additional correction for  $A_V = 0.09$  magnitudes of SMC type dust at an assumed host galaxy redshift  $z = 2.03$  has been applied. In both panels, the epochs of observation (from top to bottom) are UT 2000 March 3.50, 4.52, 6.375, 9.00, and 14.60. The corresponding times since the GRB are labeled on the plot. Solid lines connect flux densities sharing a common epoch, and dotted lines show the best-fit single power law at each epoch.

energy distributions corrected for  $A_V = 0.09$  of SMC type dust. This correction gives the minimum  $\chi^2/\text{d.o.f}$  (1.45 for 4 degrees of freedom) for the residuals of the plotted spectral energy distributions relative to the spectral slopes reported in table 3. LMC extinction does marginally worse than SMC extinction, while any amount of Milky Way extinction in the host degrades  $\chi^2$ . We have used the analytic extinction law fitting forms of Pei (1992) in deriving these estimates. Jensen et al (2000) have applied a similar analysis incorporating optical spectra as well as broadband colors. They also find a significantly better fit for SMC extinction than for either MW or LMC extinction, and derive  $A_V = 0.14 \pm 0.01$  magnitudes for the SMC model. Using our multiple epoch SEDs, we find a somewhat worse  $\chi^2/\text{d.o.f} = 1.98$  for their extinction estimate than for ours, but the two results are probably consistent within the errors, especially if there are unidentified systematic errors of  $\gtrsim 0.08$  magnitude in the photometry (see section 5).

The apparent weakness of the 2175Å feature in the extinction curve of the host galaxy is reminiscent of dust attenuation laws for actively star forming galaxies (e.g., the Magellanic Clouds [Pei 1992 and references therein] and starburst galaxies [Gordon, Calzetti, & Witt 1997]). This may be further circumstantial evidence linking GRBs to actively star forming galaxies. Alternatively, such an extinction law might be observed if GRBs preferentially destroy the small carbonaceous particles thought to be carriers of the 2175 Å feature, but this explanation would only work if much of the dust optical depth arises near the maximum radius where the burst can destroy grains (cf. Waxman & Draine 2000; Fruchter, Krolik, & Rhoads 2000).

In order to determine physical parameters of the afterglow, we need to measure the peak flux density and the locations of breaks in the afterglow spectrum (Wijers & Galama 1999). We now do this (insofar as possible) by combining our optical-IR spectral slope measurements with the submillimeter and radio data. We are looking for four numbers: The frequency  $\nu_{\text{hboxmax}}$  and flux density  $f_{\nu,\text{max}}$  at the peak in  $f_\nu$ ; the cooling frequency  $\nu_c$ , and the self-absorption frequency  $\nu_{\text{abs}}$ . The spectral slope is expected to be  $-p/2$  for  $\nu > \nu_c$ ,  $-(p-1)/2$  for  $\nu_{\text{max}} < \nu < \nu_c$ ,  $+1/3$  for  $\nu_{\text{abs}} < \nu < \nu_{\text{max}}$ , and  $+2$  for  $\nu < \nu_{\text{abs}}$  (Sari, Piran, & Narayan 1998). Here  $p$  is the power law index of electrons recently accelerated at the external shock of the expanding GRB remnant.

Extrapolating the optical-IR spectral slopes to lower frequencies, we see that a strong spectral break is required near or above the 250 GHz measurement by Bertoldi (2000) on March 4.385. The radio data from March 5.67 (Berger et al 2000) are compatible with  $f_\nu \propto \nu^{1/3}$  between 22 and 250 GHz, so we determine  $\nu_{\text{max}}$  and  $f_{\nu,\text{max}}$  by extrapolating this behavior until it intersects the extrapolation from optical-IR data (see figure 4). Using fluxes corrected for both Galactic dust and  $A_V = 0.09$  magnitude of SMC type extinction at  $z = 2.03$ , we obtain  $\log(\nu_{\text{max}}/\text{Hz}) = 11.81 \pm 0.10$  and  $\log(f_{\nu,\text{max}}/\text{mJy}) = 0.46 \pm 0.05$ , where the error bars account only for photometric errors on the data. If we do not apply any correction for host galaxy extinction, we instead obtain  $\log(\nu_{\text{max}}/\text{Hz}) = 12.16 \pm 0.08$  and  $\log(f_{\nu,\text{max}}/\text{mJy}) = 0.58 \pm 0.05$ . We can also estimate  $\nu_{\text{abs}}$  using the radio data from Berger et al (2000) that is shown in figure 4. We conservatively estimate  $3 \text{ GHz} \lesssim \nu_{\text{abs}} \lesssim 15 \text{ GHz}$  at March 5.66. Frail (personal communication) reports a best fit value of about 6.8 GHz.

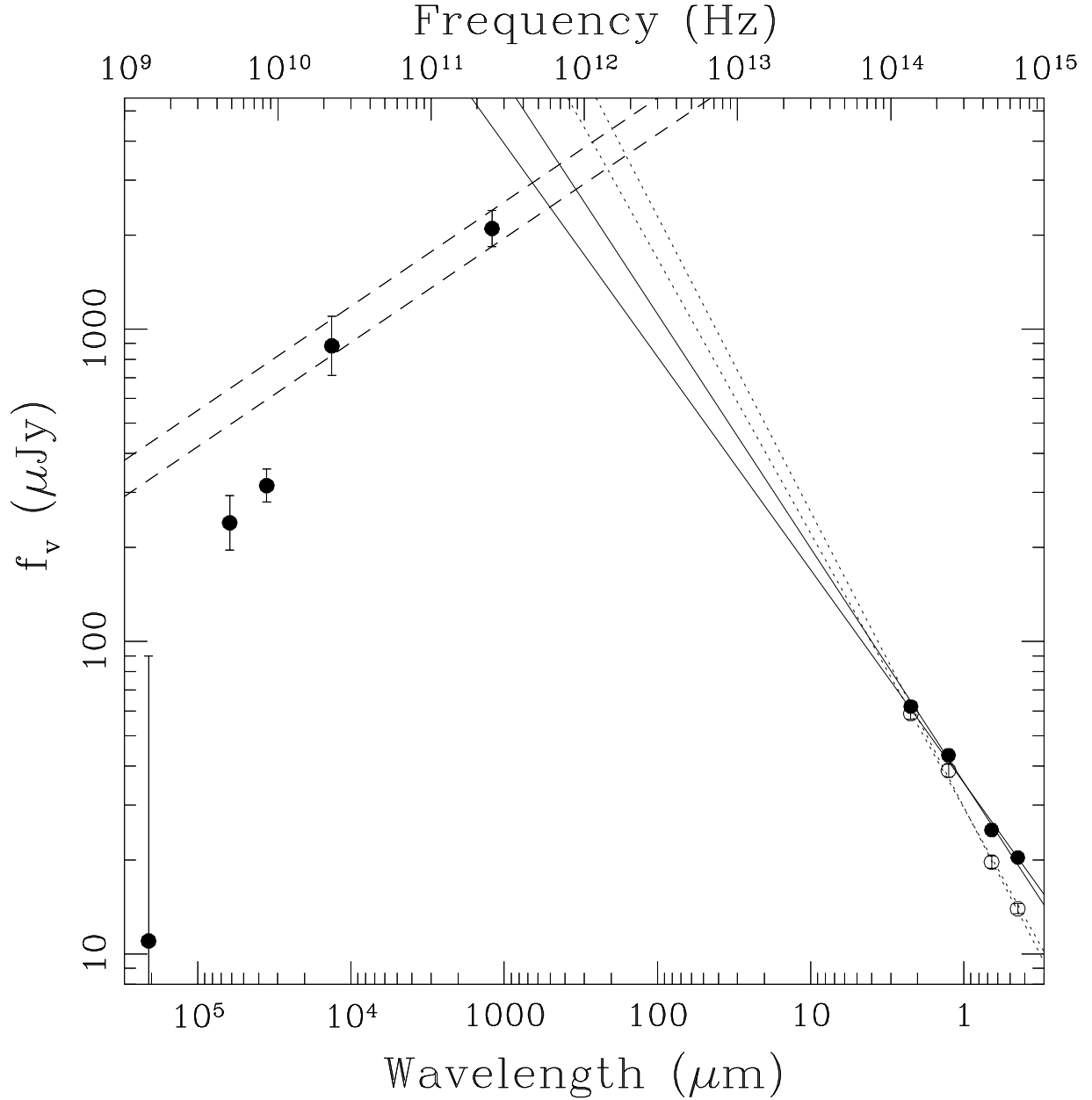


Fig. 4.— The spectral energy distribution of the GRB 000301c afterglow from 250 GHz to  $0.44 \mu\text{m}$  on UT 2000 March 4.385 (2.974 days post-GRB), and at 1.43, 4.86, 8.46, and 22.5 GHz on UT 2000 March 5.67 (4.26 days post-GRB). Filled points show the photometric data corrected for both Galactic foreground and GRB host galaxy extinction (see text). Solid lines show the  $\pm 1\sigma$  fitted power law slopes through these fully corrected optical/IR data. Open points show the optical/IR data corrected for only foreground Galactic extinction, and dotted lines show the  $\pm 1\sigma$  fitted power law slopes through these data points. Finally, dashed lines show the  $f_\nu \propto \nu^{1/3}$  slope expected between the self-absorption frequency and the peak in  $f_\nu$ .



The location of the cooling frequency  $\nu_c$  is harder to constrain, not least because it is a relatively modest break of 0.5 in spectral index and because this burst is not very well observed at X-ray wavelengths. If we take the afterglow behavior to be reasonably described by the “standard” model at the earliest observed times, then the expected behaviors are  $f_\nu \propto \nu^{-(p-1)/2}$  and  $f_\nu \propto t^{-3(p-1)/4}$  for  $\nu < \nu_c$ , or  $f_\nu \propto \nu^{-p/2}$  and  $f_\nu \propto t^{1/2-3p/4}$  for  $\nu > \nu_c$ . While this model is based on a uniform ambient medium and spherically symmetric burst, it is also valid for GRBs collimated into an angle  $\zeta$  at early times, while  $\Gamma > 1/\zeta$  (Rhoads 1997, 1999). The early time R band data (excluding the discrepant March 2.906 data point) gives  $f_\nu \propto t^{-0.71}$ . The spectral slope is  $f_\nu \propto \nu^{-0.9}$  if we omit host galaxy extinction corrections, but could be as blue as  $\nu^{-0.6}$  for moderate host galaxy extinction. Both theoretical models of electron acceleration in relativistic shocks (Bednarz & Ostrowski 1998; Gallant, Achterberg, & Kirk 1999) and experience with other afterglows give typical values  $p \approx 2.3$ . Comparable values of  $p$  are marginally consistent with the early time data if we adopt  $A_V \gtrsim 0.12$  in the host galaxy and  $\nu_c > \nu \approx 10^{15}$  Hz at  $t = 3$  days. If we require  $p \gtrsim 2$ , then  $\nu_c < 10^{15}$  Hz yields much poorer agreement. Only if we allow  $1.4 \lesssim p \lesssim 1.6$  can we find a viable model having  $\nu_c$  between optical and radio wavelengths. However, a new parameter (the upper cutoff in the electron energy spectrum) must be added to the “standard” model to accommodate  $p < 2$  and still keep a finite energy in relativistic electrons. Additionally, it is very difficult to fit the late time decay  $f_\nu \propto t^{-2.8}$  with any  $p < 2$  model; the only viable possibility we presently know of is the “naked afterglow” model of Kumar & Panaitescu (2000b). If we consider the early time K’ light curve,  $f_\nu \propto t^{-0.1}$ , and no regime under the standard model offers a self-consistent estimate of  $p$ . Overall, we regard  $p \gtrsim 2$  and  $\nu_c \gtrsim 10^{15}$  Hz around UT 2000 March 3.5 as the most plausible solution.

## 7. Physical Parameters of the Afterglow

We can use the observed spectral energy distribution of GRB 000301C to place interesting limits on some of the afterglow’s physical parameters, using the method of Wijers & Galama (1999). To do so, we assume that the afterglow is reasonably approximated by a spherical burst (or a section thereof) expanding into a uniform ambient medium up to the time of our SED measurement. Even if the light curve break is attributed to a jet, the method should work for times before the break. We take the spectrum to peak at either of the values derived above ( $\log(\nu_{\max}/\text{Hz}) = 11.81$  and  $f_{\nu,\max} = 2.9$  mJy with the host galaxy extinction correction, or  $\log(\nu_{\max}/\text{Hz}) = 12.16$  and  $f_{\nu,\max} = 3.8$  mJy with only Milky Way extinction corrections). In addition, we take  $\log(\nu_c/\text{Hz}) \geq 15$ . Using  $\nu_{\text{abs}} = 6.8$  GHz then gives “best estimate” limits of  $E > 3 \times 10^{53}$  erg  $\times \Omega/(4\pi)$ ,  $\xi_e \geq 0.11$ ,  $\xi_B \leq 1.6 \times 10^{-3}$ , and  $n \gtrsim 1\text{cm}^{-3}$ . Here  $E$  is the kinetic energy of the ejecta,  $\xi_e$  and  $\xi_B$  are the fractions of the local energy that go into relativistic electrons and magnetic fields immediately behind the expanding GRB remnant blast wave, and  $n$  is the number density of the ambient medium. We obtain limits rather than measurements because of the relatively weak constraints on  $\nu_c$  and  $\nu_{\text{abs}}$ . We have taken the most conservative pair of  $(\nu_{\max}, f_{\nu,\max})$  in deriving these limits on physical quantities. The physical quantities scale with

$\nu_{\text{abs}}$  as  $E \propto \nu_{\text{abs}}^{-5/6}$ ,  $\xi_e \propto \nu_{\text{abs}}^{5/6}$ ,  $\xi_B \propto \nu_{\text{abs}}^{-5/2}$ , and  $n \propto \nu_{\text{abs}}^{25/6}$  (Wijers & Galama 1999). If we allow  $3 \text{ GHz} \lesssim \nu_{\text{abs}} \lesssim 15 \text{ GHz}$ , and further take the one-sigma variations on  $\nu_{\text{max}}$  and  $f_{\nu, \text{max}}$  to weaken the limits, we obtain more conservative limits of  $E > 1.3 \times 10^{53} \text{ erg} \times \Omega/(4\pi)$ ,  $\xi_e \geq 0.04$ ,  $\xi_B \leq 0.02$ , and  $n \gtrsim 0.014 \text{ cm}^{-3}$ . We have used  $p = 2.3$ , but other values affect the results only weakly except for  $\xi_e$ , whose behavior approaches  $(p - 2)^{-1}$  as  $p \rightarrow 2$ . If the ill-constrained cooling frequency is substantially above  $10^{15} \text{ Hz}$  at 3 days, then the bounds on  $E$  and  $\xi_e$  rise as  $\nu_c^{1/4}$ ,  $\xi_B$  falls as  $\nu_c^{-5/4}$ , and  $n$  rises as  $\nu_c^{3/4}$  (Wijers & Galama 1999). On the other hand,  $\nu_c \ll 10^{15} \text{ Hz}$  requires  $p \sim 1.5$ . In this case the equations describing the afterglow and the inversion of measured quantities to obtain physical parameters would require new formulae.

It is interesting to compare our estimate of  $E$  with the gamma ray fluence of the burst. Jensen et al (2000) estimate a fluence of  $2.1 \times 10^{-6} \text{ erg cm}^{-2}$  in the 25 to 100 keV band and a corresponding energy of  $2.3 \times 10^{52} \text{ erg} \times \Omega/(4\pi)$ . They also report a similar fluence in the 150 to 1000 keV band, so the total energy might be  $\sim 5 \times 10^{52} \text{ erg} \times \Omega/(4\pi)$ . Thus, our most conservative limits  $E > 1.3 \times 10^{53} \text{ erg} \times \Omega/(4\pi)$  implies that  $\lesssim 0.4$  of the blast wave energy was emitted in gamma rays, while for our best estimate  $E > 3 \times 10^{53} \text{ erg} \times \Omega/(4\pi)$ , this fraction is reduced to  $\lesssim 0.15$ .

## 8. Discussion

GRB 000301c is the third burst for which a strong break in the light curve is clearly observed. Several classes of breaks are predicted by fireball models. The most basic of these are due to features in the synchrotron spectrum moving through the observed bandpass (e.g., Paczyński & Rhoads 1993; Sari, Piran, & Narayan 1998). However, this class of features predicts relatively modest changes in light curve slope, with the break occurring first at short wavelengths and evolving to longer ones. Jetlike burst ejecta, on the other hand, are expected to give strong breaks that are essentially independent of wavelength (Rhoads 1997, 1999; Sari, Piran, & Halpern 1999), and the observed breaks have generally been interpreted as evidence for collimation of the GRB ejecta (e.g., in GRB 990123, by Castro-Tirado et al 1999, Kulkarni et al 1999, Fruchter et al 1999, and Galama et al 1999; and in GRB 990510, by Stanek et al 1999 and Harrison et al 1999). A difficulty with this model is that the predicted break is quite gradual (Rhoads 1999; Panaitescu & Meszaros 1999; Moderski, Sikora, & Bulik 2000; Kumar & Panaitescu 2000a), while observed breaks are rather sharp.

The current burst is no exception. The prediction of Rhoads (1999) for the light curve around the break time for a collimated jet is

$$f_\nu \propto \frac{[t/t_b]^{-3(p-1)/4}}{(1 + 3.72 [t/t_b]^{2/5})^{5/2} * (1 + 2.07 [t/t_b]^{5/12})^{3(p-1)/5}} \quad (2)$$

where  $t_b$  is the fiducial break time defined in Rhoads (1999). The break in this predicted light curve is extremely broad, and would give  $\chi^2$  little better than a single power law in fitting the observed break in either  $K'$  or  $R$  band. The model curve is based on numerical integration of the remnant's

dynamical equations, and ignores differences in light travel time between the center and edge of the remnant, which will only smooth the break further (e.g., Moderski et al 2000; Panaitescu & Meszaros 1999).

If we ignore the issue of break sharpness and fit a collimated jet model to the observed R band light curve, we can infer the opening angle from the measured break time. To do so, we need a reasonable measurement of  $t_b$  and crude estimates of  $\Omega/E$  and  $n$ , since the inferred opening angle scales as  $(t_b^3 n \Omega/E)^{1/8}$  (Rhoads 1999). We use  $t_b = 5.1$  days and  $E = 3 \times 10^{53}$  erg  $\times \Omega/(4\pi)$ . To estimate  $n$  more precisely, we use the column density  $N(HI) \approx 10^{21.2 \pm 0.5}$  inferred from Lyman  $\alpha$  absorption (Jensen et al 2000) and estimate the linear size of the source as  $\lesssim 0.2''$  based on its nondetection in late HST images. This implies a number density  $n \gtrsim 0.4$ , consistent with our earlier estimate. Using  $n \approx 1$ , the inferred opening angle becomes  $2.5^\circ$ , or  $10^{-3}$  of the sky if the jet is bipolar.

The transition to the nonrelativistic regime has been proposed as another mechanism for light curve breaks both in this burst (Dai & Lu 2000) and others (Dai & Lu 1999). However, we do not know of a detailed calculation of the sharpness of this break, making a fair evaluation of this possibility difficult. Light travel time effects seem likely to broaden this feature to  $\delta t/t \sim 1$ , as with most other features.

A final possible cause for sharp breaks in GRB afterglow light curves is discontinuities in the ambient density distribution. Assuming that the density is a function of radius alone, a minimum timescale for breaks due to such discontinuities is  $\Delta t \gtrsim t$ , where  $t$  is the time elapsed in the observer’s frame since the burst and  $\Delta t$  the characteristic duration of a light curve feature. This duration is set by differential light travel time effects between material moving along the line of sight and off-axis material moving in direction  $1/\Gamma$ , and is a rough minimum for any afterglow light curve feature provided the ambient medium density is approximately independent of angle from the line of sight. The time required for material already in the expanding blast wave to cool by adiabatic losses is also relevant for determining the sharpness of a density discontinuity break, as is the emission from angles  $> 1/\Gamma$  off the line of sight (Kumar & Panaitescu 2000b).

If we believe that the observed  $R - K'$  variations are real, then the greatest difficulty posed by the observations of GRB 000301c is in finding a model whose light curve steepens in  $K'$  before it steepens in R. For most mechanisms, breaks will occur either first at short wavelengths (e.g. the cooling break), or simultaneously at all wavelengths (e.g. “beaming” breaks). One speculative way out is to suppose that a discontinuity in the ambient density is encountered while the cooling break is between the R and K’ filters. The predicted appearance of an afterglow at frequencies above and below this break is expected to differ qualitatively: A high frequency image would show an annular structure and a low frequency image a more nearly filled disk. This is caused by the difference in the apparent dynamical age of the remnant along the line of sight (where we see things changing quickly) and near the edge of the observed afterglow (where light travel time is larger, and we see material at an earlier and hotter stage of its evolution). (E.g., Granot, Piran, & Sari 1999.) Now,

the same variation of “lookback time” from the center to edge of the afterglow implies that we see the effect of an ambient density drop first in the middle of the afterglow, and that the fractional effect of such a discontinuity on the afterglow flux will initially be larger at long wavelengths than short ones. This mechanism can reproduce the sign of the observed effect. Detailed calculations would be necessary to see if it can approach the observed magnitude, given that the two filters are separated by only a factor of 3 in wavelength.

## 9. Summary

We present a  $K'$  band ( $2.1 \mu m$ ) light curve of the GRB 000301c afterglow, combining four epochs from a Target of Opportunity program at the NASA Infrared Telescope Facility with two additional measurements from Calar Alto (Stecklum et al 2000) and Subaru (Kobayashi et al). This light curve can be well fitted by a broken power law evolution, with a very flat early time slope ( $t^{-0.1}$ ), a steep late time slope ( $t^{-2.3}$ ), and a rather sharp break. A similar fit for R band ( $0.7 \mu m$ ) data from the literature yields steeper slopes ( $-0.7$  and  $-2.8$ ) and a later break time. A detailed analysis of the  $R - K'$  colors shows modest deviations from constant color, which are significant at the  $\sim 2\sigma$  level. These may indicate the presence of systematic errors  $\gtrsim 0.08$  magnitude due to inhomogeneous data sets. However, we believe that the likely level of such systematic errors is  $\lesssim 0.05$  magnitude, and that at least part of the color variability is likely real.

The strong break and steep late time slope in the light curves are reminiscent of GRB 990510, which has been interpreted as a collimated burst (Stanek et al 1999; Harrison et al 1999; Kumar & Panaitescu 2000a). If we fit a collimated burst model to the R band light curve, the estimated opening angle becomes  $2.5^\circ$ .

However, while a jet model can reproduce the size of the break, it does not provide a natural explanation for the observed rapidity of the break. Nor, however, do other models. Indeed, there is considerable variability in the R band light curve of GRB 000301C on time scales  $\delta t/t \leq 0.4$ . This highlights the potential for unusual temporal variability in GRB afterglows.

Fitting a standard synchrotron spectral energy distribution to the burst, we place the peak of  $f_\nu$  around  $3.4 \text{ mJy}$  at about  $10^{12} \text{ Hz}$  ( $300 \mu m$ ). The dominant uncertainty in this measurement is the correction for extinction in the GRB host galaxy. Random errors are  $\approx 0.10$  dex in  $\nu_{\text{max}}$  and  $0.05$  dex in  $f_{\nu, \text{max}}$ , while the correction for host galaxy extinction is uncertain at perhaps twice this level. These strong constraints on the  $f_\nu$  peak are possible because of the precise optical-IR spectral slope measurements afforded by  $K'$  observations.

Combining the measured spectral peak with constraints on the cooling frequency and self-absorption frequency, we infer that the blast wave energy required to power this afterglow was  $E > 3 \times 10^{53} \text{ erg}$  if isotropic. The corresponding efficiency of gamma ray production in the burst was  $\lesssim 0.15$ .

It is a pleasure to thank the NASA IRTF director and staff for making this observing program possible. Special thanks are due to Bob Joseph, for arranging the target of opportunity mechanisms; Bill Vacca, for help with observing strategies; and Bill Golisch, Paul Fukumura-Sawada, and Dave Griep for observing. We also thank Sylvio Klose, Dale Frail, and Naoto Kobayashi for useful communications. JER's work is supported by an Institute Fellowship at STScI.

## REFERENCES

- Bednarz, J, & Ostrowski, M 1998, *Phys. Rev. Lett.* 80, 3911
- Bernabei, S., Bartolini, C., Di Fabrizio, L., Guarnieri, A., Piccioni, A., & Masetti, N. 2000, *GCNC* 599
- Berger, E., et al 2000, to appear in *ApJ*; astro-ph/0005465
- Bessell, M. S., 1990, *PASP* 102, 1181
- Bhargavi, S. G., & Cowsik, R., *GCNC* 630
- Bertoldi, F. 2000, *GCNC* 580
- Campins, H., Rieke, G. H., & Lebofsky, M. J. 1985, *AJ* 90, 896
- Casali, M. & Hawarden, T. 1992, *JCMT-UKIRT Newsletter* 4, 33
- Castro, S. M., et al 2000, *GCNC* 605
- Castro-Tirado, A. J., et al 1999, *Science* 283, 2069
- Dai, Z. G., & Lu, T. 1999, *ApJ* 519, L155
- Dai, Z. G., & Lu, T. 2000, astro-ph/0005417
- Fruchter, A., et al 2000, *GCNC* 602
- Fruchter, A., et al 2000, *GCNC* 627
- Fruchter, A., et al 2000, *GCNC* 701
- Fruchter, A., et al 1999, *ApJ* 519, 13
- Fruchter, A. S., Krolik, J. H., & Rhoads, J. E. 2000, submitted to *ApJ*
- Fukugita, M., Shimasaku, K., & Ichikawa, T. 1995, *PASP* 107, 945
- Fynbo, J. P. U., et al 2000, *GCNC* 570
- Galama, T. J., et al 1999, *Nature* 398, 394
- Gallant, Y., Achterberg, A., & Kirk, J. G. 1999, *A&AS* 138, 549
- Gal-Yam, A., Ofek, E., Maoz, D., & Leibowitz, E. M. 2000, *GCNC* 593
- Garnavich, P., Barmby, P., Jha, S., & Stanek, K. 2000a, *GCNC* 573
- Garnavich, P., Barmby, P., Jha, S., & Stanek, K. 2000b, *GCNC* 581

- Gordon, K. D., Calzetti, D., & Witt, A. N. 1997, *ApJ* 487, 625
- Granot, J., Piran, T., & Sari, R. 1999, *ApJ* 513, 679
- Gunn, J. E., & Stryker, L. L. 1983, *ApJS* 52, 121
- Halpern, J. P., Mirabal, N., & Lawrence, S. 2000a, GCNC 578
- Halpern, J. P., Mirabal, N., & Lawrence, S. 2000b, GCNC 582
- Halpern, J. P., Mirabal, N., & Lawrence, S. 2000c, GCNC 585
- Halpern, J. P., & Kemp, J. 2000, GCNC 604
- Harrison, F. A., et al 1999, *ApJ* 523, 121
- Henden, A., et al 2000, GCNC 583
- Jensen, B. L., et al 2000, submitted to *A&A*; astro-ph/0005609
- Kobayashi, N., Goto, M., Terada, H., Tokunaga, A. T., et al 2000a, GCNC 577
- Kobayashi, N., Goto, M., Terada, H., Tokunaga, A. T., et al 2000b, GCNC 587
- Kulkarni, S. R., et al 1999, *Nature* 398, 389
- Kumar, P., & Panaitescu, A. 2000a, astro-ph/0003264
- Kumar, P., & Panaitescu, A. 2000b, astro-ph/0006317
- Leggett, S. & Denault, T. 1996, “NSFCam User’s Guide,” version 3
- Madau, P. 1995, *ApJ* 441, 18
- Masetti, N., et al 2000, to appear in *A&A*; astro-ph/0004186v2
- Moderski, R., Sikora, M., & Bulik, T. 2000, *ApJ* 529, 151
- Mujica, R., Chavushyan, V., Zharikov, S., & Tovmassian, G. 2000, GCNC 597
- Panaitescu, A., & Meszaros, P. 1999, *ApJ* 526, 707
- Paczynski, B., & Rhoads, J. E. 1993, *ApJ* 418, L5
- Pei, Y. C. 1992, *ApJ* 395, 130
- Rhoads, J. E. 1997, *ApJ* 487, L1
- Rhoads, J. E. 1999, *ApJ* 525, 737
- Sagar, R., Mohan, V., Pandey, S. B., Pandey, A. K., & Castro-Tirado, A. J. 2000, to appear in *BASI*; astro-ph/0004223
- Sari, R., Piran, T., & Narayan, R. 1998, *ApJ* 497, L17
- Sari, R., Piran, T., & Halpern, J. 1999, *ApJ* 519, L17
- Schlegel, D. J., Finkbeiner, D. P., & Davis, M., 1998, *ApJ* 500, 525
- Smette, A., et al 2000a, GCNC 603
- Smette, A., et al 2000b, *ApJ*, submitted; astro-ph/0007202

- Smith, D. A., Hurley, K., & Kline, T. 2000, GCNC 568
- Stanek, K. Z., Garnavich, P. M., Kaluzny, J., Pych, W., & Thompson, I. 1999, ApJ 522, L39
- Stecklum, B., Klose, S., Fischer, O., et al 2000, GCNC 572
- Veillet, C., & Boer, M. 2000a, GCNC 575
- Veillet, C., & Boer, M. 2000b, GCNC 588
- Veillet, C., & Boer, M. 2000c, GCNC 598
- Veillet, C., & Boer, M. 2000d, GCNC 610
- Veillet, C., & Boer, M. 2000e, GCNC 611
- Wainscoat, R. J., & Cowie, L. L. 1992 AJ 103, 332
- Waxman, E., & Draine, B. T. 1999, astro-ph/9909020
- Wijers, R. A. M. J., & Galama, T. J. 1999, ApJ 523, 177

UT date	$t$	Filters	Slope (none)	Slope (MW)	Slope (MW + host)	Slope (R-K)
3.50	2.09	B,R,J,K'	$-0.905 \pm 0.026$	$-0.789 \pm 0.026$	$-0.596 \pm 0.026$	$-0.722 \pm 0.038$
4.385	2.974	B,R,J,K'	$-1.032 \pm 0.032$	$-0.911 \pm 0.033$	$-0.709 \pm 0.032$	$-0.901 \pm 0.052$
4.52	3.11	B,R,J,K'	$-1.049 \pm 0.035$	$-0.927 \pm 0.036$	$-0.727 \pm 0.035$	$-0.932 \pm 0.051$
6.375	4.964	UV,R,K'	$-1.18 \pm 0.10$	$-1.03 \pm 0.10$	$-0.83 \pm 0.10$	$-0.99 \pm 0.15$
9.00	7.59	R,K'	$-0.78 \pm 0.11$	$-0.69 \pm 0.10$	$-0.54 \pm 0.10$	$-0.69 \pm 0.10$
14.60	13.19	B,R	$-1.64 \pm 0.37$	$-1.44 \pm 0.37$	$-1.07 \pm 0.36$	n/a

Table 3: Spectral slopes  $d \log f_\nu / d \log(\nu)$  of the GRB 000301c afterglow at selected epochs. Column sub-headings indicate the type of extinction correction applied, starting with none, then correcting for Milky Way extinction only, and finally for both Milky Way extinction and host galaxy extinction. The last column gives the slope measured using the R and K' filters alone, corrected for Milky Way extinction only, to isolate the time evolution of the burst from possible systematic differences among filters. Host galaxy extinction corrections assume  $A_V = 0.09$  at  $z = 2.03$  with a Small Magellanic Cloud extinction law (Pei 1992).